Numerical Simulation of the VAR Process with calco*soft*®-2D and its Validation

G. Reiter[a], V. Maronnier[b], C. Sommitsch[a], M. Gäumann[b], W. Schützenhöfer[a], R. Schneider[a]

[a] Böhler Edelstahl GmbH & Co KG, 8605 Kapfenberg, Austria
[b] Calcom SA, 1015 Lausanne, Switzerland

Abstract

Numerical simulation of remelting processes has become more and more popular over the last 2 decades. The reasons for the increasing interest of both university and industry is obvious: to get a better understanding and thus to optimise the processes. Böhler Edelstahl GmbH & Co KG has been using the commercial software calco*soft*®-2D to simulate the VAR process for 2 years.

The software calco*soft*®-2D is FEM based and solves the heat flow equation in 2-dimensional systems. Convection and transport are accounted for by coupling the heat conduction equation with the Navier-Stokes equation. For the numerical simulation of the VAR process a special module has been developed in calco*soft*®-2D to take into account the magneto-hydrodynamic effects caused by the high current density in the liquid pool region and its influence on the pool flow regimes occurring.

Practical experiments were carried out on ingots made of alloy 718. Pool profiles were investigated for different melt rates on 410mm (16") and 510mm (20") ingots. Additionally, the temperature distribution along the mould surface was measured in order to carry out inverse calculations to get the heat flow boundary conditions for the simulation. Additionally, inverse calculations were carry out to get the heat flow boundary conditions for the simulation.

The basis of remelting simulations is the understanding of the heat balance of the system. Calculations and estimations of the boundary conditions including the heat fluxes, the shrinkage gap formation and the additional heat due to arc radiation are described. Simulations were carried out calculating heat flow, transport and fluid flow problems.

The influence of the magneto-hydrodynamic effect on the fluid flow; the comparison of simulations and experimental results; and the dependence of the remelting process on different ingot dimensions are discussed.

1 INTRODUCTION

The VAR-process has become a standard remelting facility to produce special alloys during the last decades. Böhler Edelstahl GmbH&CoKG is actually operating 3 VAR-furnaces up to 950mm ingot diameter, which are mainly used for the production of special iron and nickel alloys. A very high process understanding is necessary, to meet the demands, that are mad on this alloys, which shall be extended by the aid of solidification simulation. A program has been started with the aim to establish VAR-simulation with the commercial software calco*soft*®-2D and to develop the software further for this application.

The difficulties to simulate VAR processes are directly linked to the wide range of physical and chemical phenomena present and often coupled in such remelting processes [2]. A comprehensive numerical simulation would incorporate fluid flow, heat and mass transfer, electromagnetic effects, solidification (including grain nucleation and growth) and macro-segregation. The modeling of heat transfer, fluid flow and solidification including grain nucleation and growth and macro-segregation is already done in the commercial finite element software calco*soft*®-2D [6], dedicated to casting processes. Moreover, the software calco*soft*®-2D contains hot tearing, an induction heating model which allows magnetic stirring to be modeled. An inverse solver for the determination of boundary conditions and material properties is also available. However, due to the geometry of VAR furnace and its power supply, a new axisymmetric electromagnetic solver, including both Lorentz's forces and Ohm's heating calculation, has been developed in calco*soft*®-2D to simulate VAR process.

2 THE MATHEMATICAL MODEL

The model is based on the numerical solution of Navier-Stokes, Fourier and steady-state Maxwell equations. Heat and Fluid flow models are detailed in [6]. The electromagnetic model is different to that used by the authors [1,3,4,5]. First, the electric potential and the electric current density are computed as it is done in [8]

but taking the influence of the velocity into account. Then, the magnetic field is computed from an original model [7]. Finally, the Lorentz's forces and Ohm's heating can be evaluated.

The following assumptions have been made. The ingot is treated as axisymmetric, i.e. in two dimensions using cylindrical coordinates, see figure 2.1. The arc, created by the circulation of a direct current between the cathode and the mold, is assumed to be diffuse, i.e. without short-circuit. A stationary regime is considered in the simulations. According to these assumptions, only the upper part of the ingot is simulated with solid transport. Appropriate boundary conditions are applied to represent the arc and mass transfer from the cathode.
Fig. 2.1: Axisymmetric situation of a VAR process.
The equations being solved are listed below.

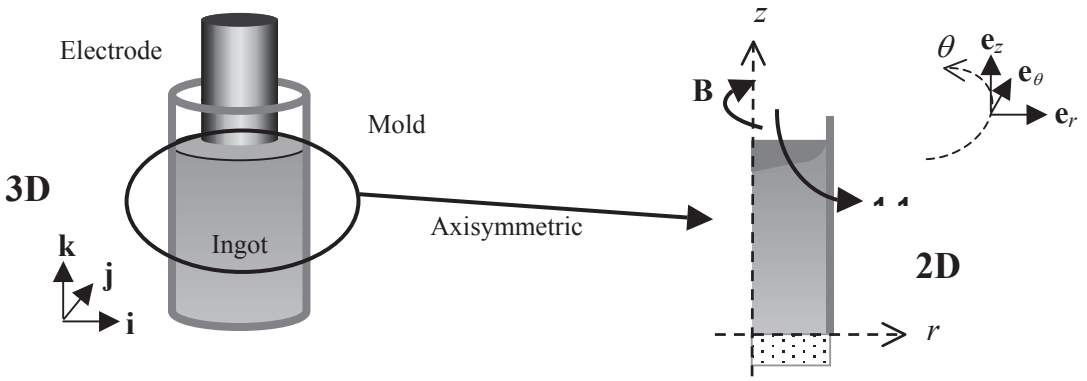

Figure 2.1: 2D model of the VAR process

2.1 Energy conservation

The energy equation to be solved is:

$$\frac{\partial H}{\partial t} + \mathbf{v}_s \cdot \nabla H + \rho c_p (\mathbf{v} - \mathbf{v}_s) \cdot \nabla T - \operatorname{div}(\kappa \cdot \nabla T) = \frac{\mathbf{J} \cdot \mathbf{J}}{\sigma}, \tag{2.1}$$

where H is the volumic enthalpy, $\mathbf{v}_s$ is the transport velocity of the solid, ρ the density, c_p the specific heat, κ the thermal conductivity and T the temperature. The average velocity $\mathbf{v}$ is defined by $\mathbf{v} = f_s \mathbf{v}_s + f_l \mathbf{v}_l$, where f_s is the fraction of solid, f_l the fraction of liquid and $\mathbf{v}_l$ the velocity of the fluid. The source term represents the Ohm's heating, where σ is the electrical conductivity and $\mathbf{J}$ the electric current density. Furthermore, the conversion into variation of temperature and volume fraction is made according to a microscopic model of solidification.

2.2 Continuity and momentum equations

Incompressible Newtonian viscous fluids are considered. The mass conservation is:

$$\operatorname{div} \mathbf{v} = 0. \tag{2.2}$$

Taking into account the interaction between the solid phase and the liquid phase in the mushy zone and using the Boussinesq approximation, the momentum equation is written as follows:

$$\rho \frac{\partial \mathbf{v}}{\partial t} + \frac{\rho}{f_l} (\mathbf{v} \cdot \nabla) \mathbf{v} - 2\mu \operatorname{div}(\varepsilon(\mathbf{v})) + f_l \nabla p = f_l \rho \mathbf{g} \beta (T - T_0) + f_l \mathbf{J} \times \mathbf{B} - f_l \frac{\mu}{K} (\mathbf{v} - \mathbf{v}_s), \tag{2.3}$$

where p is the pressure of the fluid, μ the viscosity, $\mathbf{g}$ the gravitational acceleration, β the thermal expansion coefficient and T_0 a reference temperature. The term $\varepsilon(\mathbf{v})$ corresponds to the rate of deformation tensor. The term $\mathbf{J} \times \mathbf{B}$, where $\mathbf{B}$ is the magnetic induction field, represents the Lorentz's forces and the last term of the right hand side represents the damping of the fluid in the mushy region, due to the solid, where K is the local permeability of the mushy region. In the liquid, the permeability is infinite and the source term vanishes.

2.3 Electromagnetic model

A quasi steady-state electromagnetic model has to be computed for each time step. The circulation of a direct current between the cathode and the mold creates a magnetic field, which must satisfy the following steady-state Maxwell's equations in the whole space:

$$\mathbf{rot}\, \mathbf{B} = \mu_0 \mathbf{J}, \tag{1.4}$$

$$\mathbf{rot}\, \mathbf{E} = 0 \Rightarrow \mathbf{E} = -\nabla \varphi, \tag{1.5}$$

$$\operatorname{div} \mathbf{B} = 0, \tag{1.6}$$

where μ_0 is the magnetic permeability, φ the electric potential and **E** the electric field. Moreover, the Ohm's law is applied in the set of conductors:

$$\mathbf{J} = \sigma \left(\mathbf{E} + \mathbf{v} \times \mathbf{B} \right). \tag{1.7}$$

First, combining equations (1.5) and (1.7) and having the divergence of **J** equal to zero, the electric current conservation equation can be written as follows:

$$-\operatorname{div} (\sigma \nabla \varphi) = -\operatorname{div} (\sigma \, \mathbf{v} \times \mathbf{B}). \tag{1.8}$$

Second, applying the Ohm's law with the previous value of the electric potential, the electric current density is then computed as follows:

$$\mathbf{J} = \sigma \left(-\nabla \varphi + \mathbf{v} \times \mathbf{B} \right). \tag{1.9}$$

Finally, according to the first assumption, the magnetic induction is defined by $\mathbf{B} = B_\theta(r,z)\,\mathbf{e}_\theta$ satisfying automatically equation (1.6). As B_θ is bounded inside a conductor, it is possible to define explicitly B_θ from the relation (1.4), as it is done in [1]. However, the magnetic field is computed in the following way. B_θ fulfils equation (1.4) in cylindrical coordinates, that is:

$$\frac{\partial}{\partial r}(rB_\theta) = \mu_0 r J_z \quad \text{and} \quad \frac{\partial}{\partial z} B_\theta = -\mu_0 J_r, \tag{1.10}$$

where J_z and J_r are the components of **J** according to $\mathbf{e}_r$ and $\mathbf{e}_z$. Defining $\psi = rB_\theta$, these equations represents the components of the gradient of ψ according to r and z. Taking the divergence, with r and z as Cartesian coordinates, of the gradient of ψ, it yields

$$\Delta_{rz}\, \psi = \operatorname{div} \mathbf{f} = \operatorname{div} \begin{bmatrix} \mu_0 r J_z \\ -\mu_0 r J_r \end{bmatrix}. \tag{1.11}$$

The following boundary conditions are always prescribed to have a well-posed problem: $\psi = 0$ on the axis of symmetry and the natural condition $\nabla_{rz}\, \psi \cdot \mathbf{n} = \mathbf{f} \cdot \mathbf{n}$, otherwise, where **n** is the outward normal of the boundary.

Equations (1.1) for heat, (1.2)-(1.3) for fluid and (1.8) for electric potential require appropriate initial and boundary conditions discussed in the next section.

3 CALCULATIONS

The VAR process is characterised by an axisymmetric geometry, so all calculations are carried out in a 2D axisymmetric system. The model for the simulation contains the ingot and the copper mould; the electrode and the electric arc are not directly considered by the geometry. Heat flow, transport of the solid phase, fluid flow and the magnetodynamic effects in the pool due to the melt current are taken into account by the calculations.

Trials were carried out for two different dimensions, a 410mm (16") ingot and a 510mm (20") ingot, both made of Alloy 718. Geometry (mould and electrode dimension) and process parameters (melt rate and melt current) correlate to that used for industrial production. A adequately fine mesh was used with an increasing number of elements at the top and ingot-mould-interface.

Starting from fictitious start conditions, *where* the temperature of the whole ingot is set to 1300°C and the mould temperature is set to 36°C, the heat balance of the system is calculated until stationary conditions are reached. A sufficiently high number of time steps have to be calculated to guarantee this situation. Transient process phases (e. g. melt rate changes or falling in of material) and process parts, that are transient by nature (e. g. hot topping or the start phase), are not taken into consideration.

3.1 Thermal model of the ingot

The thermal boundary conditions play an important part in the prediction of the temperature distribution and the pool profile in the steady state of the VAR process. The following main assumptions have been made in the numerical model. Figure 1 shows the heat fluxes during VAR, where heat flux 1 is the incoming energy, heat flux 2 is radiation from annulus to the top, heat flux 3 stands for the heat transfer from the ingot to the cooling water and heat flux 4 and 5 represents the radiation from the electrode and the arc, respectively, to the mould.

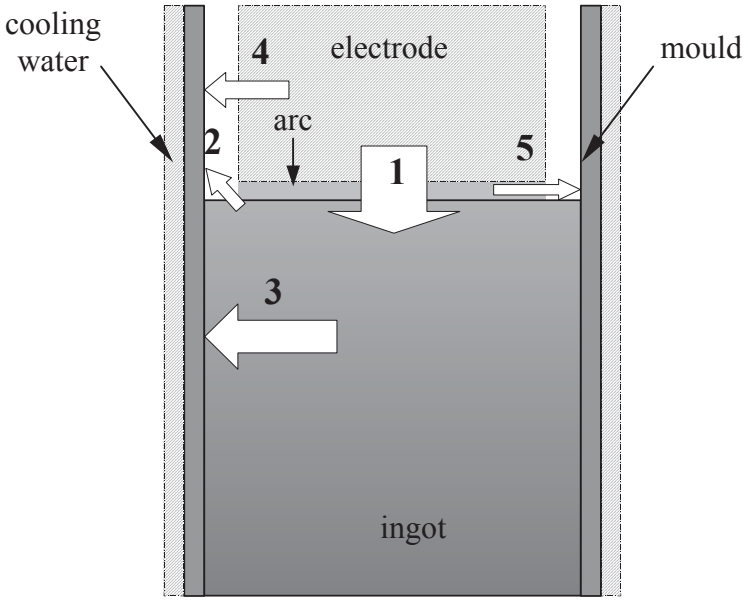

Figure 3.1: Heat fluxes during VAR

3.1.1 Heat flux 1

The total incoming energy, which consists of the energy of the droplets and the energy coming from the radiation of the electric arc is represented by a constant temperature of the pool surface, which is given by the liquidus temperature and a superheating, and constant flow of material according to the melt rate. The latter is estimated by the product of x and P where x is the fraction of arc energy that goes into the melt and P is the power of the arc per electrode cross-section.

3.1.2 Heat flux 2

Different fill ratios lead to different annuli between the electrode and the mould. The heat transition at the annulus is governed by an arbitrarily set constant temperature.

3.1.3 Heat flux 3

There can be distinguished between a small contact zone of the liquid melt and a gap between the solidified ingot and the mould due to shrinkage, respectively (fig. 1c). The transition temperature contact vs. gap was set to a temperature T_{crit} below the solidus temperature. Heat transfer h_{gap} between the ingot and the mould was calculated by

$$\begin{aligned} h_{gap} &= h_{cont} \qquad if\ T > T_{crit} \\ h_{gap} &= h_r + h_g \quad else \end{aligned} \tag{3.1}$$

where h_{cont} is the heat transfer coefficient in case of contact,

$$\mathrm{h_r} = \varepsilon\sigma\frac{\mathrm{T}^4 - \mathrm{T_m}^4}{\mathrm{T} - \mathrm{T_m}} \tag{3.2}$$

is the heat transfer coefficient due to radiation, T is the temperature of the ingot surface, T_m is the temperature of the mould (inside), ε is the emissivity of the material and σ is the Stefan-Boltzman constant.

$$h_g = \frac{\lambda_g}{r_i\left[\ln\left(\frac{r_m}{r_i}\right) + \frac{g_i}{r_i} + \frac{g_m}{r_m}\right]} \tag{3.3}$$

is the conductive heat transfer coefficient using the analogy of conduction through the rarefied gas between coaxial cylinders which is valid for very low pressures [1], where λ_g denotes the thermal conductivity of gas, r the radius and g the temperature jump distance of the mould (subscript m) and the ingot (subscript i),

respectively. For sufficiently large gaps, h_g can be approximated by λ_g/gap. This allows to take into consideration the presents of gas, e.g. He, in the shrinkage gap.
The heat transfer in the copper mould h_m is given by the thermal conductivity divided by the thickness of the mould.
The heat transfer between the mould and the cooling water h_w is based on the analogy of the heat transfer coefficient for turbulent flow in an annular tube [2]

$$\mathrm{St}\left(\mathrm{Pr}\right)^{\frac{2}{3}} = 0.023\left(\mathrm{Re}\right)^{-0.2} \tag{3.4}$$

which depends on the Stanton number *St*, the Prandtl number *Pr* and the Reynolds number *Re*.
Thus the overall heat transfer coefficient *h* between the ingot and the cooling water can be derived by

$$h = \frac{1}{\frac{1}{h_{gap}} + \frac{1}{h_m} + \frac{1}{h_w}}. \tag{3.5}$$

Fig. 3.1 shows the dependence of the overall heat transfer coefficient and the different contributions on the gap width. At small gap widths the heat transfers between the ingot and the mould and between the mould and the cooling water are of the same order of magnitude. For gap widths larger than 1mm only the heat transfer between mould and ingot are from major influence. The constant overall heat transfer coefficient in case of contact is also inserted into the figure.

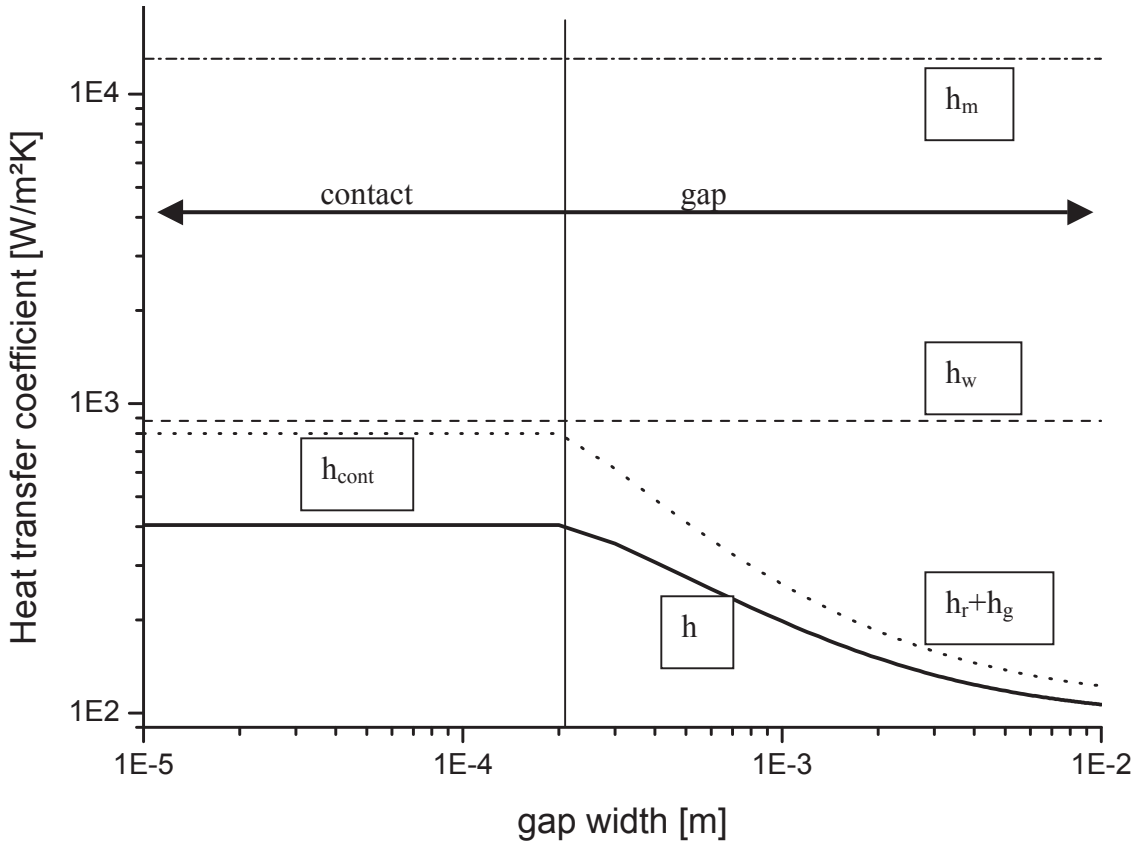

Fig. 3.1: Heat transfer coefficients in [W/m²K] between the ingot and the cooling water as a function of the gap width in [m] for Alloy 718: ingot diameter=510mm, He pressure=15Torr, temperature=1273K. The transition from contact to gap was set to 0.2mm for this calculation.

To estimate the gap width, additional calculations were made with the FEM-code DEFORM™. This programme was developed for the calculation of metal forming processes, thus the liquid pool of the VAR can´t be described. Therefore the axisymmetric model was simplified in the following way: The real shape of the formed liquid pool, which was measured by a macro etched longitudinal test specimen, gives the geometry of the ingot top. A fixed temperature - the measured solidus temperature due to cooling - was chosen as thermal boundary condition. Furthermore there is a heat transfer between the ingot and the water cooled copper plate at the bottom. This heat transfer coefficient was calculated by inverse modelling and is equal to 800 W/m²K.

The heat transfer between the ingot and the copper mould was modelled as follows: At the top, where the ingot touches the mould, there is a contact boundary condition. In the case of contact there is a friction coefficient equal 0.3 and a heat transfer coefficient equal 800 W/m^2K. After gap formation the heat transfer consists of radiation and heat conduction by helium, which fills the gap. An emissivity of 0.4 and a constant heat transfer coefficient of 100 W/m^2K were chosen for this calculations.

It is interesting to know the whole length profile of the gap. As a result the ingot height was fixed with 2 meters. The result of the described calculation is given in figure 3.2. It shows the gap as a function of the vertical distance from the liquid pool. The gap opens very quickly within the first 500 mm below the pool. This is due to high temperature gradients in vertical as well as in radial direction. More below the thermal gradient of the ingot is very low therefore the ongoing thermal shrinkage, which causes the gap formation, is very slow. The maximum gap of the 510 mm ingot lies between 4.5 and 5.0 mm.

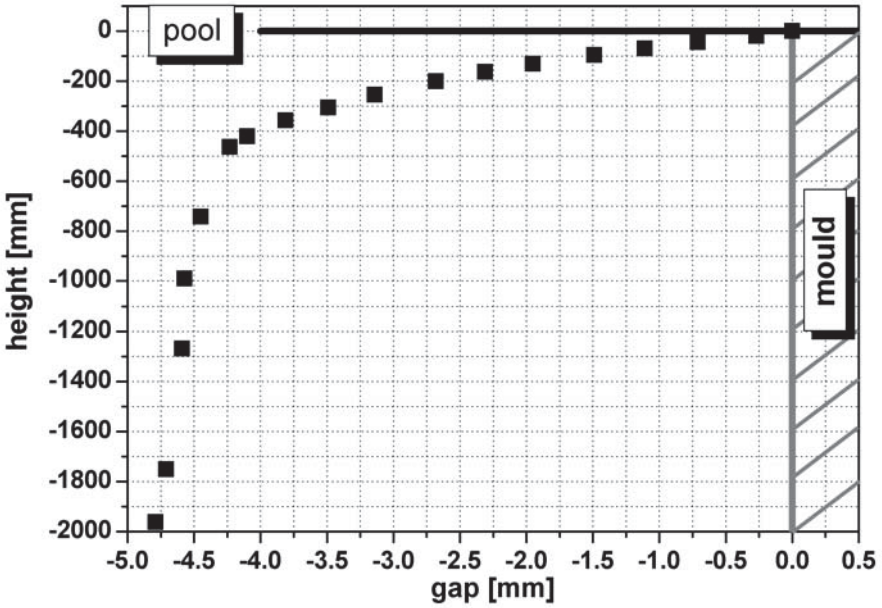

Figure 3.2: Shrinkage gap formation as a function of distance from pool

3.1.4 Heat fluxes 4 and 5

In addition to that mentioned above, heat fluxes appear, which have no direct influence on the ingot. Radiation from the electric arc and the electrode directly to the mould appears.

3.2 Material data

All material data for Alloy 718 and for the mould material (copper), are taken from published data bases.

4 RESULTS

4.1 Simulation results

The main results that are obtained are the temperature distribution, the distribution of the fraction of solid in the ingot and the fluid flow in the liquid pool. Figure 4.1 shows the results of a 510mm ingot. The temperature distribution on the left hand shows a superheated layer on the pool surface right below the electrode and a very steep gradient near to the mould in the upper region of the ingot. The fraction of solid distribution on the right hand in principal shows a typical pool profile of a VAR. The liquidus and solidus line are supposed the be set at a fraction of solid of 0,98 and 0,02, respectively. On the right upper corner of the ingot, against the typical pool profile, almost no solid shelf is formed in this region.

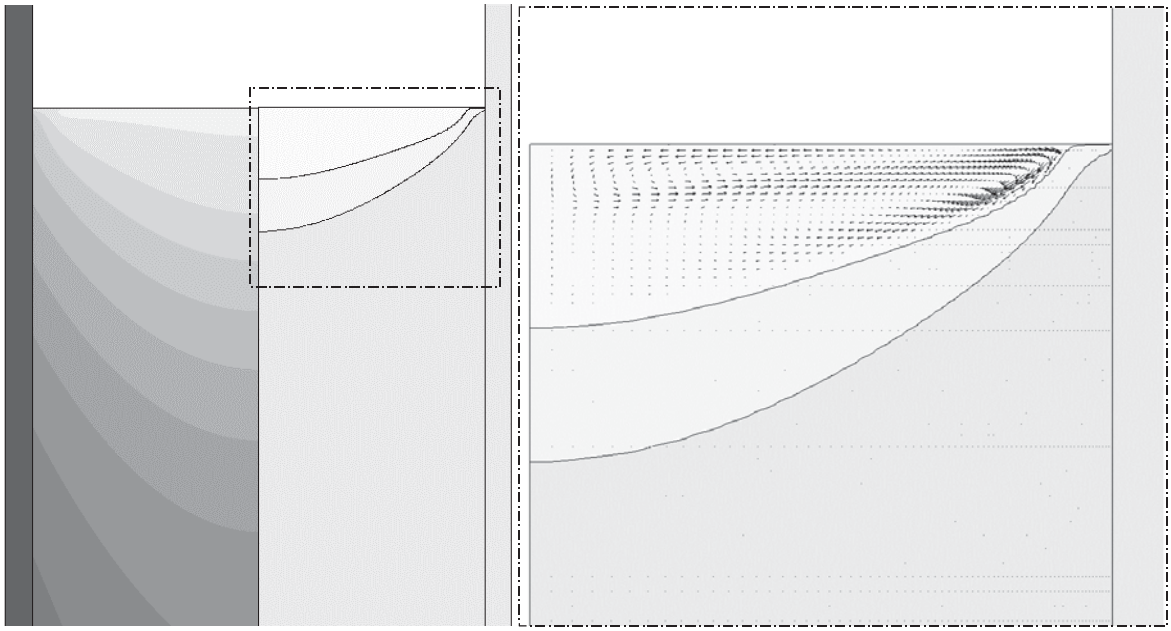

Figure 4.1: Temperature distribution, pool profile and flow pattern of a 510mm ingot simulation; alloy 718

The magnification of the pool region illustrates the fluid flow in the liquid phase. Two different flow regime become visible: one in the upper pool region near to the pool surface which borders directly on the second one in the lower region of the pool. In the upper region the flow is signed through a downwards flow in the centre of the ingot, whereas in the lower region, the fluid flows upwards at the centre.

A comparison between fluid flow calculated with and without taking into account the magnetodynamic effects is shown in figure 4.2. Against the flow conditions described above, which can be seen on the left hand (Figure 4.2), the flow on the right hand is marked through one flow regime with a flow direction and intensity similar to that in the low region of the pool at the left hand.

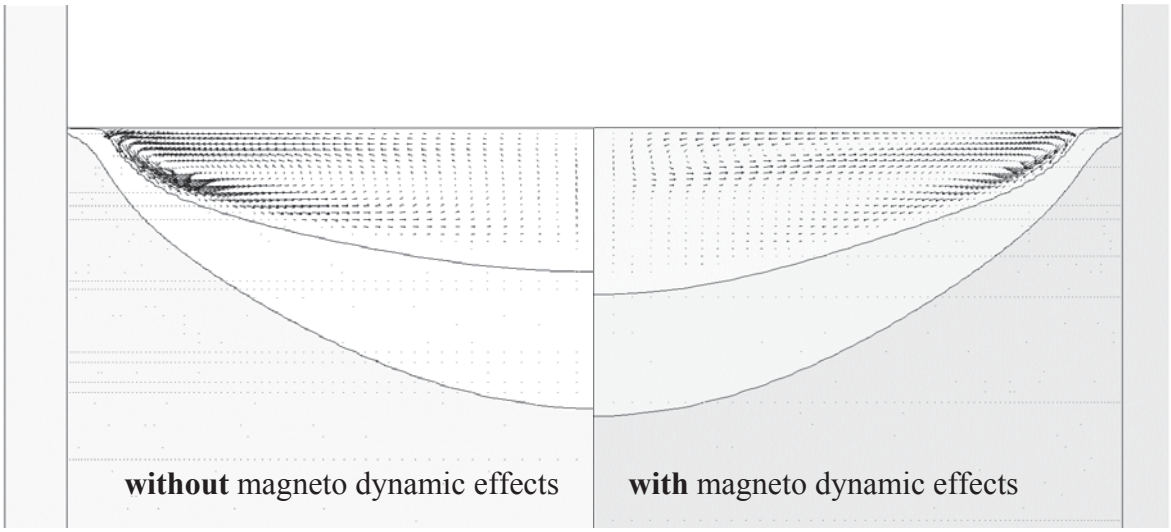

Figure 4.2: Pool profiles and flow patterns with and without magneto dynamic effects of 510mm ingots; alloy 718

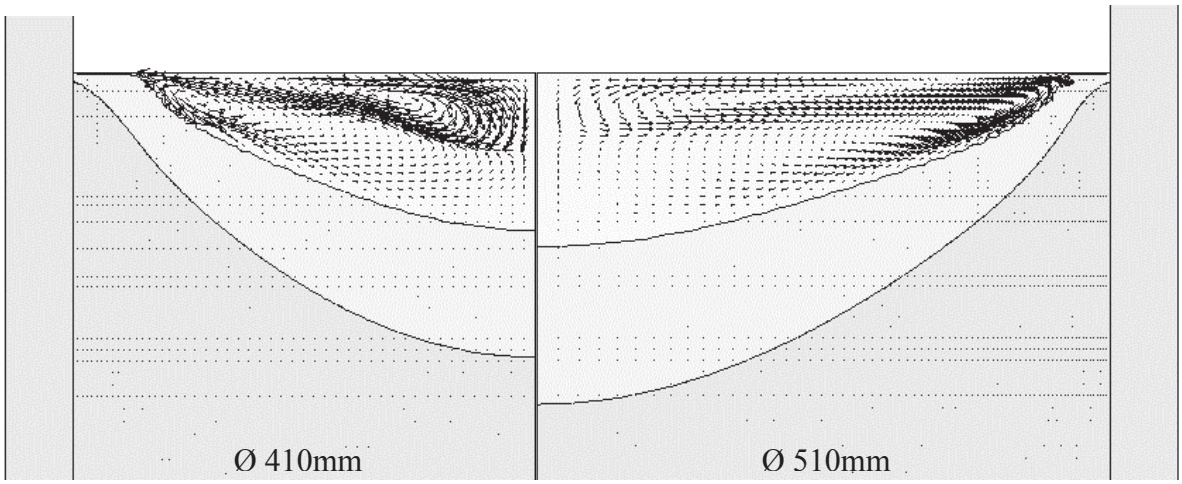

Figure 4.3: Simulated pool profiles and flow patterns of 410mmand 510mm ingots

A decrease of ingot diameter, which can be correlated to a increase of current density, leads to a higher flow velocity in the upper swirl. Figure 4.3 compares the different flow regimes appearing in the 410mm and in the 510mm ingot. Besides the swirl itself gets larger.

4.2 Comparison between measured pool and simulation

The pool profile of ingots, produced on production plants at the special steel plant at Böhler Edelstahl GmbH & CoKG in Austria, where measured to compare the simulation results with the measured pool profiles and to verify the validity of the boundary conditions and assumptions that have been mad. For this purpose, ingots were mad without hot toping and horizontal slices were taken from the top. These slices were etched and the pool profile was estimated from the microstructure, assuming, that the transition from columnar to the fine equiaxed grains signs the solidus line. This is illustrated in Figure 4.4

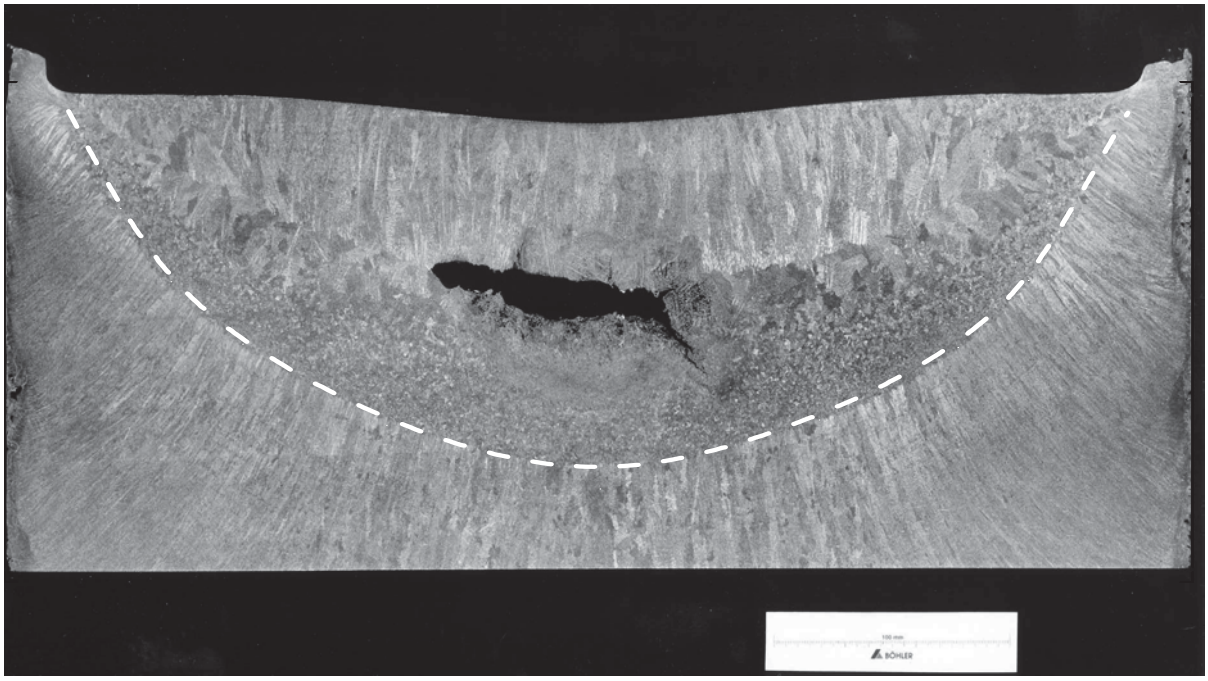

Figure 4.4: Microstructure of a 510 mm ingot remelted without hot topping and pool profile; alloy 718

The comparison between the measured and the calculated pool profile for a 410mm (16” ingot) is shown in Figure 4.5. It can be noticed, that the simulated profile is parallel to the measured one, the pool depth of the simulation is slightly lower. Near to the mould, the difference between both is evident in so far, as the slope of the solidus line is steeper at the measured one ending in the formation of the solid shelf, which is not possible at the simulation (as mentioned above).

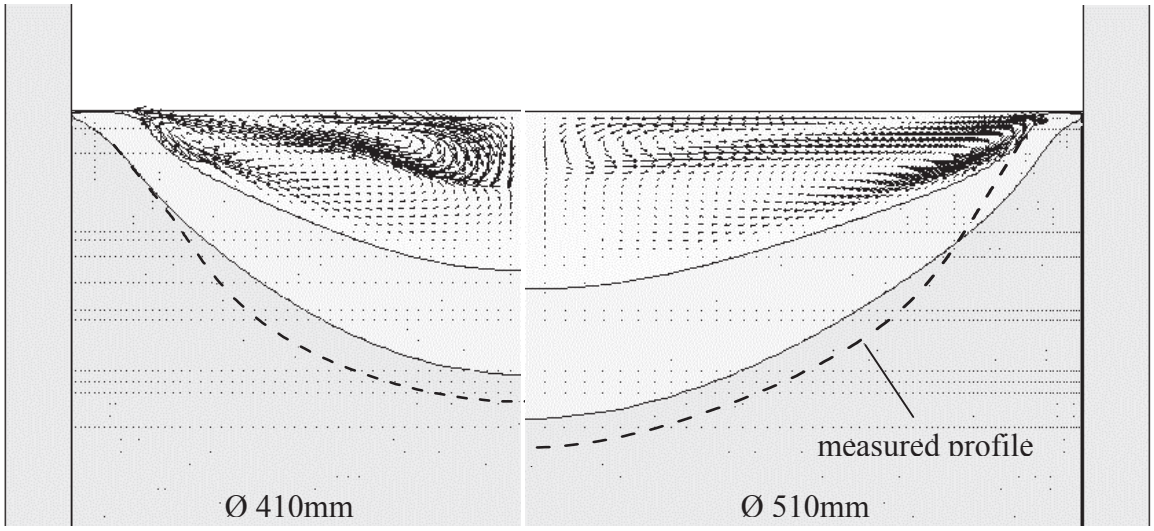

Figure 4.5: Comparison of simulation and measured pool profile for 410mm and 510mm ingot

The 510mm (20") ingot result (Figure 4.5) looks a little different. In the inner region of the ingot, the pool depth and the profile of the simulation correlates quite well with the measurement, whereas the difference in the shelf region is a little higher than at the smaller ingot.

5 DISCUSSION AND OUTLOOK

Generally, the temperature distribution and the pool profile is typical for the VAR process and can be found in literature. The untypical pool profile near the mould is connected with the boundary conditions on boundary 2. On this boundary, a liquid layer has to be established in the program to avoid calculation errors. Various trials showed, that this has no big influence on the pool depth and on the flow pattern.
The different flow regimes can be related to the different acting forces (Figure 4.3): on top of the pool, where the current density is very high, the flow is mainly driven by Lorenz forces. This lead to the observed flow pattern. Further below the surface, where the current density decreases, the flow regime is mainly driven by Buoyancy forces. Figure 4.2 shows the difference between the flow pattern calculated without MHD module, only Buoyancy driven flow, and the flow pattern taking also into account the influence of the Lorenz forces. Figure 4.2 also visualises, how the MHD module is working and the great influence, even on the pool profile, it has. The higher current density occurring in the 410mm ingot lead to an increase of Lorenz forces, a large region of Lorenz driven flow and higher flow velocity.

The comparison between measured and simulated pool profiles indicates, that in principal there is a good correlation between the pool profiles for the 410mm, as well as for the 510mm ingot. Furthermore, this shows, that the assumption and calculations for the boundary conditions are valid in general and not only "customized" to one dimension.

There are some further steps planed for the future. At first, a measurement of the local solidification time will be carried out to compare the results with the values, that can be derived from the simulation to carry out a more accurate validation of the model. On this base, calculations of different parameter sets will be carried out, with the goal to understand the influence of the various process parameters on the melting behaviour during steady state. Additionally, the simulation will be extended to microstructure and segregation prediction. Moreover, the simulation of the solidification behaviour of other alloys during VAR shall be done.